Indonesian Journal of Electrical Engineering and Computer Science
Vol. 43, No. 1, July 2026, pp. 63~77
ISSN: 2502-4752, DOI: 10.11591/ijeecs.v43.i1.pp63-77

Advanced state machine-sliding mode current control energy management for multi-source DC microgrid

Hamza Rezigue[1], Mabrouk Khemliche[1], Samia Latreche[1], Badreddine Kanouni[1], Hamza Khemliche[2]
[1]Department of Automatic Laboratory, Automatic and Intelligent Systems, Setif-1 University, Sétif, Algeria
[2]CRTI Centre in Industrial Technologies- Cheraga 16014, Algiers, Algeria

Article Info

Article history:

Received Jan 6, 2026
Revised Jun 2, 2026
Accepted Jun 27, 2026

Keywords:

DC microgrids
Energy management
Proton exchange membrane fuel cell
Sliding mode control
State machine control

ABSTRACT

This work addresses effective power management in a multi-source DC microgrid. An innovative energy management technique utilizing a state machine control (SMC) integrated with a sliding mode current control (SMCC) has been developed. This approach offers advantages through its equitable distribution of power among sources, storage devices, and demand loads, thereby optimizing the flow rate, discharge, and charge cycles of energy storage devices; additionally, it improves the response time of PEMFC power across various states in comparison to a conventional PI controller. The SMC-SMCC has proposed nine scenarios, categorized into three state of charge (SOC) situations, to fulfill a predetermined set of parameters for the operation of the DC microgrid. Simulation studies conducted with a precise model in MATLAB/Simulink have demonstrated that the proposed SMC-SMCC is proficient in achieving effective power sharing, rapid DC link voltage control in terms of stability, and maintaining the SOC within its constraints; additionally, the SMC-SMCC exhibits a quicker response time compared to conventional SMC-PI.

Corresponding Author:

Badreddine Kanouni
Department of Automatic Laboratory, Automatic and Intelligent Systems, Setif-1 University
Sétif, Algeria
Email: badreddine.kanouni@univ-mail.dz

1. INTRODUCTION

Microgrids utilizing energy from renewable resources (RERs) are garnering heightened interest across multiple industries, including industry, automotive applications, maritime vessels, seaports, and satellites. This curiosity is propelled by technological innovations, elevated efficiency in renewable energy, the creation of novel hybrid storage components, and proficient power balancing facilitated by powerful power control techniques [1]-[3]. A centralized production system with interconnected microgrids can facilitate the utility grid's operation as a smart grid. These MGs deliver agile power generation, effectively mitigating grid uncertainty and peak demands [4]. Moreover, microgrids can enable decentralized smart power generation, either as AC microgrids that deliver AC power compatible with the utility grid, or as DC microgrids that provide DC power for DC loads or energy storage systems.

Most DC MGs get their energy from renewable sources, such as photovoltaic, wind, and generators, and provide it to DC loads and storage devices. These systems use modern power electronic converters, strong controllers, and better power management methods to make sure that power is always available.

The architecture of DC microgrids offers advantages such as a reduced number of converters, enhanced efficiency, diminished losses, absence of skin effect, and simplified control, as reactive power and frequency fluctuations are not concerns within the system [5]. Atmospheric variations influence the substantial nonlinear power produced by solar and wind energy systems. Maintaining a reliable power supply is problematic due to the unpredictability of renewable energy sources such as wind and solar, compounded by the irregular patterns of energy demand throughout the hour, day, and season.

In the event of power outages, energy storage devices might provide renewable electricity, reducing the severity of these problems. Due to the wide variety of energy storage systems (ESS) features and characteristics, no single technology can address all of the important application requirements. This includes things like electric power and energy densities, discharge rate, load profile, and more. Consequently, batteries emerge as a favorable choice, and exhibit a high energy storage density; however, they demonstrate a low power density.

Although they are essential, deep charge-discharge cycles actually reduce the lifespan of batteries when used frequently [6]. An increasing number of people are considering merging fuel cells with contemporary energy storage technologies in order to increase the systems' power density and dynamics. Because the hybridization technique optimizes the fuel-cell system, the ultimate result is better fuel efficiency and overall performance. It uses the supplementary properties of batteries to its advantage.

A powerful energy management strategy (EMS) that intelligently distributes power loads across multiple energy sources is pivotal to the successful implementation of this optimization process. Developing an EMS necessitates a meticulous equilibrium between enhancing fuel efficiency and ensuring the optimal operation of each energy source within its designated parameters. Furthermore, reducing the EMS's influence on the hybrid power system's entire life cycle is essential. Extensive research literature exists on energy management solutions for fuel-cell hybrid power systems. State machine control (SMC) is a methodology employed in the electrical domain, recognized for its direct, rule-based framework. SMC depends on the information and insights derived from heuristic or empirical prior experiences. The effectiveness of this approach depends on your familiarity with how the various parts of the system work [7]. Another method is named the rule-based fuzzy logic energy management system. This system efficiently allocates power using membership functions and IF-THEN rules. This technique is easy to tune for optimal operation and robust to measurement imprecision and component fluctuations. However, the fuzzy logic controller's (FLC) performance depends on IF-THEN rule development, which requires expertise and experience. The field uses rule-based fuzzy logic energy management systems extensively. This system distributes power effectively using membership functions and IF-THEN rules [8].

Recent advancements indicate that energy management utilizing classical PI controllers has become a significant strategy. Proportional-integral (PI) controllers monitor critical performance metrics, including battery state of charge (SOC), supercapacitor voltage, and DC-bus voltage [9]. In contrast to various other strategies, the implementation of PI controllers does not require specialized expertise, and they can be easily tuned in real-time to improve tracking performance, effectively addressing steady-state load demands. Sliding mode current controllers (SMCC) have recently garnered interest as a viable alternative to conventional PID controllers for the design of stabilizers aimed at mitigating power oscillations. The SMCC ler exhibits notable advantages, including robustness and ease of implementation. Furthermore, it exhibits superior performance, characterized by rapid response and minimal current ripples, when compared to the PI controller. Additionally, it does not necessitate a load voltage sensor, unlike the predictive controller [10].

The topic of energy management for hybrid systems has advanced significantly in recent years. Numerous strategies have been put forth to improve these systems' dependability and efficiency. Li *et al.* [11] combine Q learning with deterministic rules to mitigate current fluctuations; however, the extensive training requirements and model dependency pose challenges for real-time applications. A fuzzy rule-based strategy employs fuzzy logic to address uncertainties and imprecise information [12]. Cui *et al.* [13] presents an approach utilizing fuzzy logic to maintain the fuel cell within a high-efficiency zone while accommodating rapid demand changes. In their comparison of several control systems, Luciani and Tonoli [14] single out fuzzy logic as the one that can increase fuel cell efficiency for low-load cycles by as much as 33%. For a hybrid system that incorporates fuel cells, batteries, and supercapacitors, a type-2 fuzzy technique is employed in [15]. Stability and efficiency are both enhanced by this method's rigorous control. In order to optimize the distribution of energy in real time, Zhang *et al.* [16] combine fuzzy adaptive management with driving mode recognition through a neural network. Using the prairie dog optimizer (PDO), a novel load frequency control (LFC) methodology that combines FLC with tilted fractional order integral derivative with fractional filter (TFOIDFF) controllers was presented in [17]. A two-area hybrid power grid that incorporates electric vehicles (EVs), superconducting magnetic energy storage (SMES), and a unified power flow controller (UPFC) is used in the study to assess the controller's performance This paper offers a novel contribution to overcoming the limitations in existing research on microgrid energy management, specifically addressing challenges related to complexity, scalability, and the need for real-world validation. Table 1 summarized comparative of various existing control methods and the proposed state machine sliding mode current control (SMC–SMCC) approach. Form above the shortcomings of existing EMS approaches are listed as follows: PI controllers: the authors thank the reviewer for this recommendation in response. Insufficient dynamic performance for quick load transients. A rigid gain arrangement demonstrates insufficient robustness to parameter variability. Degradation of performance in nonlinear operational conditions. Both overshoot and settling time are aspects that require consideration.

FLC ttechnical deficiencies: substantial dependence on regulations defined by experts and membership functions, lack of a methodical tuning strategy, performance sensitive to variations in operational conditions. As the system becomes increasingly complex, the rule base expands significantly.

Reinforcement learning (RL) EMS: substantial computational requirements during training, significant data requirements for convergence, assurances of stability are complex., Constraints on the deployment of real-time systems within embedded systems. The proposed SMC–SMCC method ensures swift finite-time convergence, considerable resilience to system nonlinearities and parameter uncertainties, reduced computational requirements, and minimized chattering, making it highly suitable for real-time energy management in DC micro grid systems. To enhance power flow in the hybrid DC microgrid and overcome the limitations of the PI controller, we propose a new SMCC. A comparative analysis between the proposed controller and the PI controller will be performed to verify effectiveness.

2. CONTRIBUTION AND SIGNIFICANCE

This is the inaugural combination of SMC with SMCC for PEMFC-based DC microgrids, resulting in enhanced dynamic responsiveness and superior SOC regulation. This work primarily contributes by introducing a state machine sliding mode current control (SMC-SMCC) to address the issues associated with control approaches for DC-MG applications, which is presented as follows:

- The SMC-SMCC technique enhances the performance and efficacy of the examined DC-MG system.
- The implementation of EMS utilizes SMC-SMCC for the regulation of the DC-DC boost in the PEMFC system.
- The SMC-SMCC represents a novel strategy that diverges from the conventional SMC-PI methodology and demonstrates remarkable efficiency.
- The SMC SMCC guarantees efficient power-flow regulation between the generator and the load under various operational conditions.
- Substantially enhanced the response time relative to the utilization of PI control, also substantially enhancing the resilience of the control system.

This paper is organized as follows: section 3 delineates the system architecture and the modelling of various sources. In section 4 delineates energy management solutions employing the state machine in conjunction with SMCC. In section 5 analyses the simulation outcomes, while section 6 represents the conclusion of his study.

Table 1. Comparison between different methods and the proposed SCM-SMCC

	Advantages	Drawbacks	Comparison with SCM-SMCC
PI control	Elementary execution; minimal computational costs	Parameter adjustments affect sensitivity	Improved robustness and faster convergence are two benefits offered by SMCC.
Fuzzy logic control	Deals with nonlinearities in the absence of a clear model; adaptive actions	Heuristic rule design; tuning intricacy; potential steady-state error	SMCC provides stability through mathematics, whereas fuzzy logic depends on principles derived from experience.
Predictive control (MPC)	Optimizes performance while handling restrictions and future forecasts	Relies on precise prediction models; heavy computational	While SMCC is quicker and uses less computing power, it does not handle constraints or optimization explicitly.
SCM-SMCC (Proposed)	Reaction time is minimal, robustness against uncertainty is high, and convergence is time bound.	Chattering and potential switching losses; needed model-based uncertainty limits	Improves dynamic response and disturbance rejection but requires mitigation of practical implementation issues

3. CONFIGURATION OF THE MULTISOURCE SYSTEM

Figure 1 shows the design of the DC microgrid. The photovoltaic (PV) system, proton exchange membrane fuel cell (PEMFC), and battery connect to the DC bus through DC–DC converters, while DC loads connect directly. A (DC–DC) buck-boost converter links the solar panel to the DC bus, a (DC–DC) boost converter connects the PEMFC to the DC bus, and a bidirectional DC–DC converter connects the battery.

3.1. Photovoltaic modelling

Various mathematical models of photovoltaic systems were developed to clarify the properties and behaviors arising from the physical manufacturing of photovoltaic cells. The P-V and I-V characteristics of the PV system show fluctuations depending on external variables. The photovoltaic module is assembled by connecting many individual cells in parallel, and this same construction process is used to create a photovoltaic generator or array. The current generated by a specific cell can be obtained from the electrical circuit shown in Figure 2 which is represents by (1) [18], [19].

$$I_{pv} = I_{ph} - I_d \left[exp \frac{q(V_{pv} - I_{pv}R_s)}{nkT} - 1 \right] - \frac{V_{pv} + I_{pv}R_s}{R_{sh}} \quad (1)$$

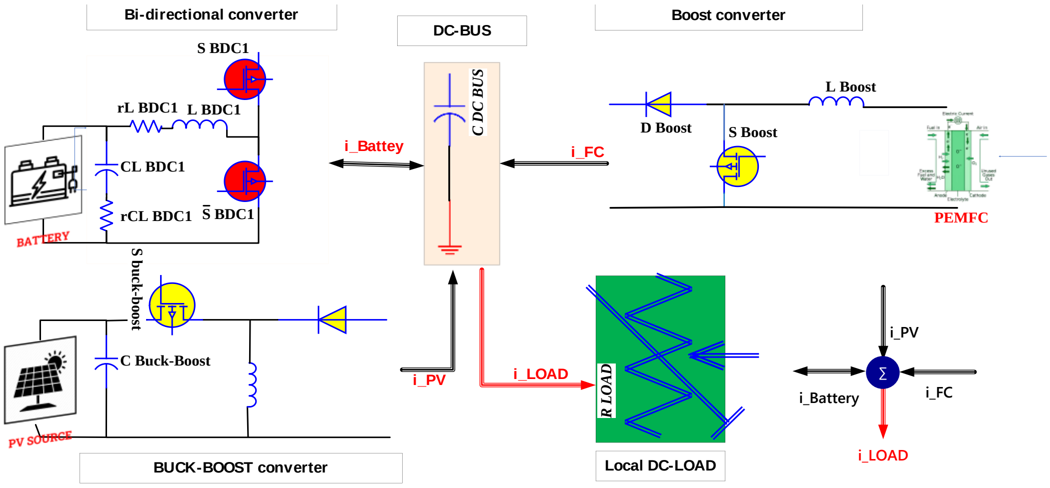

Figure 1. Architecture of the multi-source system

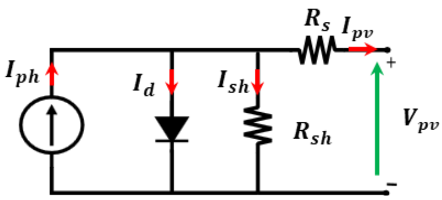

Figure 2. Solar cell circuit

According to (1), constructing a photovoltaic (PV) module involves connecting many PV cells in series (Ns) and parallel (Np); the PV module's configuration is described in (2) [20]:

$$I_{pv} = N_p I_{ph} - N_p I_d \left[exp \frac{q\left(V_{pv} - (\frac{N_s}{N_p}) I_{pv} R_s\right)}{N_s nkT} - 1 \right] - \frac{V_{pv} + (\frac{N_s}{N_p}) I_{pv} R_s}{(\frac{N_s}{N_p}) R_{sh}} \quad (2)$$

3.2. Modelling of PEMFC

The intricate, nonlinear behavior of PEMFCs is influenced by cell temperature, pressure, humidity, and current density. The performance, economic viability, and stability of PEMFCs in many applications rely on accurate modelling of these characteristics. PEMFCs transform hydrogen and oxygen into electrical energy via electrochemical reactions within the cell membrane. The resultant voltage-current (V-I) characteristics are nonlinear and influenced by activation, ohmic, and concentration losses, necessitating specialist modeling techniques for accurate representation. The total output voltage of the PEMFC stack (V_s), the electrical circuit of PEMFC is shown in Figure 3 [21].

$$V_s = n_s(E_{Nrs\_cell} - V_{act\_cell} - V_{ohm_{cell}} - V_{con_{cell}}) \quad (3)$$

The E_{Nrs_cell} represents the cell's reversible voltage, defined as the potential measured under open circuit circumstances when the cell is in thermodynamic equilibrium without any load applied as shown in (4), Furthermore V_{act_cell}, $V_{ohm_{cell}}$, and $V_{con_{cell}}$ represented the activation, ohmic, and concentration losses, as shown in (5)-(7).

$$E_{Nrs\_cell} = 1.229 - 8.5 \times 10^{-4}(T_{fc} - 298.15) + 4.3085 \times 10^{-5} \times T_{fc} \times [ln(P_{H_2}) + (1/2)\, ln(P_{O_2})] \quad (4)$$

$$V_{act\_cell} = -\left[\varsigma_1 + \varsigma_2 T_{fc} + \varsigma_3 T_{fc} ln\left(\frac{P_{O_2}}{5.08\times10^6 exp\left(\frac{-495}{T_{fc}}\right)}\right) + \varsigma_3 T_{fc} ln(I_{fc})\right] \quad (5)$$

$$V_{ohm\_cell} = I_{fc}(\Omega_c + \Omega_m) \quad (6)$$

$$V_{con\_cell} = -\beta\, ln\left(1 - \frac{J}{Jmax}\right) \quad (7)$$

The pressure of hydrogen is denoted as P_{H_2}, the pressure of oxygen as P_{O_2}, and the temperature of the cell as T_{fc}. The operational current is I_{fc}, and the semi-empirical coefficients are $\varsigma_{1,2,3,4}$. Ω_c represents the concentration resistance, while Ω_m denotes the ohmic membrane resistance. While (J) denotes the actual current density of the cell.

3.3. Modeling of battery storage

The battery demonstrates significant potential for renewable energy storage in multi-source systems, owing to its low self-discharge rate, rapid dynamic response, and high energy density. Figure 4 depicts a circuit analogous to the battery employed for the assessment of its functionality. Furthermore, the voltage is modulated nonlinearly according to the charging method to sustain the battery's capacity at an acceptable performance level. When the discharge phase is in progress, the voltage is determined by applying the formula that is presented below:

$$V_B = V_0 + R \times i - K \times (\frac{Q}{Q-it})i + A \times exp(B_B \times it) \quad (8)$$

The SOC of the battery can be calculated using the following equation:

$$SOC = SOC_0 - \frac{1}{Q}\int idt \quad (9)$$

In this context, R_B represents the internal resistance of the battery, V_0 denotes its open-circuit voltage, i_B indicates the charging current, K refers to the polarization voltage, C_B signifies its capacity, A_B corresponds to the exponential voltage, and B_B is also used to denote the exponential capacity.

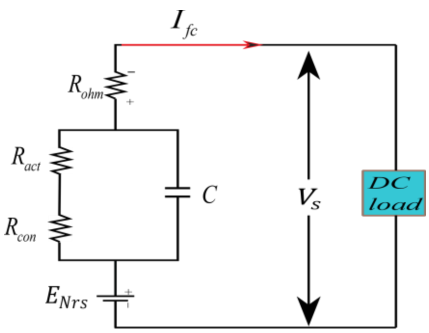

Figure 3. PEMFC electrical circuit

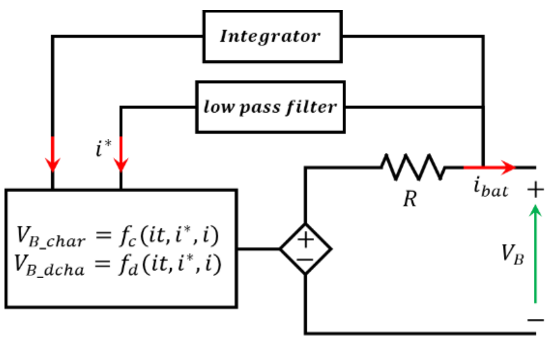

Figure 4. Circuit of battery storage

4. ENERGY MANAGEMENT CONTROL FOR MULTI-SOURCE SYSTEM

The design of the DC microgrid presented in this work is seen in Figure 1. The multi-source system delineated in this study is uncomplicated to create and execute. When power generation fails to meet demand or exceeds the required power. The photovoltaic power is monitored via a boost converter utilizing the available solar potential and regulated with maximum power point tracking under standard conditions. The EMS transitions to chosen modes after addressing the local power balance and determining the appropriate operating mode.

The control structure employs current regulation loops for BDCs that connect local buses with BESS, and utilizes SMCC for the boost converter that links local buses with PEMFC. The load power discrepancies at the local (10):

$$P_{ld} = V_{dcb} \times I_{dcb} = V_{dcb} C_{dcb} \left(\frac{dV_{dcb}}{dt}\right) \quad (10)$$

The DC link is suggested to be a capacitor. After defining all the fundamental models, we integrated the power sources in accordance with the DC bus design. The current is supplied by each source collected on the bus. The computation for the DC link current is as follows:

$$I_{dcb} = I_{pv} + I_{pemfc} \pm I_{batt} \quad (11)$$

The BDC monitors the local bus voltage to rectify imbalanced power via the BES's charge/discharge mechanism employing a dual-loop configuration. The PI regulator of the outer bus voltage loop calculates a current I_{PI} to assess the precision of the proposed energy management strategies. The BES converter is designed for local bus voltage management and load demand correction by mitigating power deficits. In (12) and (13) illustrate how the voltage loop compensates for the reference current IPI during charge and discharge modes, which is calculated by the MSEMS unit.

$$\Delta I_{BSS} = (I_{pi} - I_{BSS}) \quad (12)$$

$$I_{pi} = (K_p + \frac{K_i}{p})(V_{DC}^{*} - V_{DC}) \quad (13)$$

The BDCs' supplementary PWM commands are generated by converters' PWM generators, while the inner current loops monitor the setpoint and provide the averaged duty cycle signals.

4.1. State machine SMCC

The energy management system is seen as the control level for the system in this technique for managing energy, which involves dividing the net power of the system between the fuel cell system and the battery pack. Maintaining steady and cost-effective functioning of this DC microgrid requires an energy management plan. This paper presents an energy management technique utilizing sliding mode control, which offers numerous advantages: Sliding mode provides enhanced flexibility and reduced variability in comparison to a PI controller; Diverse control measures can be utilized; and It improves the inherent reliability of the system.

4.2. State machine control

The SMC technique is a traditional rule-based approach for managing energy systems within a microgrid. The SMC strategy in this microgrid has 9 states categorized into three SOC states, as seen in Table 2. The three SOC states are categorized as high, normal, and low. The reference power of the fuel cell is established based on the battery SOC range and the system's net demand power (Pnet). Concurrently, the following constraints have been taken into account: Pload, Pbatt, and Ppv represent the real-time measured load demand power and the output power of the photovoltaic generation system, respectively; Pfcmin, Pfcmid, and Pfcmax denote the minimum, optimum, and maximum output power of the fuel cell system.

Table 2. State machine control decisions

SOC	P_{net}	p_{fc}^{*}	State
SOC_{min}	$P_{net} < P_{min}$	P_{mid}	1
	$P_{min} \leq P_{net} < P_{mid}$	$P_{mid} + P_{min}$	2
	$P_{mid} \leq P_{net} < P_{max}$	P_{max}	3
SOC_{mean}	$P_{net} < P_{min}$	P_{max}	4
	$P_{min} \leq P_{net} < P_{mid}$	P_{min}	5
	$P_{mid} \leq P_{net} < P_{max}$	P_{mid}	6
SOC_{Max}	$P_{net} < P_{min}$	$P_{max} - P_{mid} - P_{min}$	7
	$P_{min} \leq P_{net} < P_{mid}$	$P_{mid} - P_{min}$	8
	$P_{mid} \leq P_{net} < P_{max}$	P_{min}	9

4.3. Sliding mode current control

The function of SMCC is to implement the I_fc to monitor the I_{fc}^{*}provided by the SMC decisions table. The control architecture is predicated on a DC–DC boost converter structure [22]-[25]. A boost converter is a DC–DC power electrical device that elevates the input voltage to a higher output voltage. This is seen in the figure. Five The converter's functionality is comprehended by examining its two switching states. Figure 5 illustrates the operating modes of the proposed DC–DC boost converter. Specifically, Figure 5(a) shows the switch-on (On) condition, while Figure 5(b) presents the switch-off (Off) condition. The corresponding equivalent circuits for each operating mode are also illustrated in the respective subfigures. The following equations describe each operating mode.

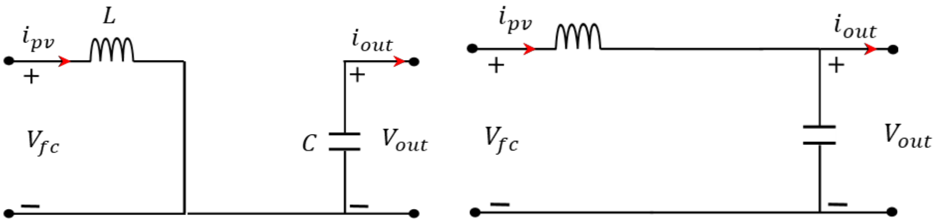

(a) (b)

Figure 5. DC-DC boost circuit: (a) switch on and (b) switch off

We can describe the boost converter model equations as follows:

$$\begin{cases} L\frac{dI_{fc}}{dt} = \left[V_{fc} - (1-S)V_{out}\right] \\ C\frac{dV_{dc}}{dt} = \left[(1-S)i_{fc} - i_{out}\right] \end{cases} \tag{14}$$

For the SMCC, the surface is specified as follows:

$$\psi = I_{fc-ref} - I_{fc} \tag{15}$$

In order to ensure that the PEMFC current I_{fc} follows the SMC decisions I_{fc-ref}, the control S can be described as [9]:

$$S = \frac{1}{2}(1 - Ksign(\psi)) \tag{16}$$

K in the SMC-SMCC law is selected to satisfy the reachability condition and to guarantee finite-time convergence of the system trajectories to the sliding surface, which is presented in (16).

Its value is determined such that it compensates for the worst-case bound of lumped uncertainties, including modeling errors, parameter variations, and external disturbances. K is not chosen excessively large, in order to limit control effort and mitigate chattering effects.

To confirm the control structure, the stability of the current loop is examined using the Lyapunov function; the Lyapunov condition is specified as [10]:

$$V = \frac{1}{2}\psi^2 > 0 \quad if\ \psi \neq 0 \tag{17}$$

One way to express the derivative of (14) using (15) is as:

$$\psi^* = I_{fc-ref} - I_{fc} = -\frac{V_{fc}}{L} - \frac{(1-S)V_{out}}{L} - I_{fc}^* \tag{18}$$

Furthermore, the expression for the derivative of V can be calculated using (18).

$$\begin{cases} V^{``} = \psi\left(-\frac{V_{out}}{2L} - -\frac{sign(S)V_{out}}{2L} + \frac{V_{fc}}{L} - \dot{I}_{fc-ref}\right) < 0 \\ 0 < V_{fc} - L\dot{I}_{fc-ref} < V_{out} \end{cases} \tag{19}$$

The use of the signum function to send the control signal S has a big problem: the chattering phenomenon, which is an infinite switching frequency that is hard to achieve [10]. To solve this problem and allow for an appropriate frequency change, the signum function must be replaced by a hysteresis band.

The discontinuity of sliding mode control may result in increased switching frequency of power electronic equipment. An increased switching frequency or more assertive control transitions may result in heightened switching losses, greater thermal stress, and diminished efficiency.

5. RESULTS AND DISCUSSION

This section examines the efficacy of the suggested energy management system, SMC-SMCC, utilized for the regulation of the multisource system. Different load values are applied to the system, and its performance is assessed in each of the nine modes, which are separated into three scenarios. Throughout the whole performance analysis, the load profiles and PV irradiance are regarded as being identical in all three scenarios. While Table 3 presents the global system, parameters utilized in the simulation. The load profile and the photovoltaic irradiance profiles are depicted in the Figure 6. The load profile fluctuates between 1,000 and 2,000 W, whereas the PV irradiance profile ranges from 700 to 1,000 as presented in Figure 7.

Table 3. Global system parameters

Photovoltaic panel (PV)		PEMFC		Battery	
Maximum power (Pmax)	60 W	ς_1	-0.944	Capacity	*14 Ah*
Maximum voltage (Vmpp)	17.1 V	ς_2	$3.5x10^{-03}$	Battery response time	0.1 s
Maximum current (Impp)	3.5 A	ς_3	$-4, 7.8x10^{-08}$,	/	/
Panel in series (Ns)	5	ς_4	$, 1.96x10^{-04}$	/	/
Panel in parallel (Np)	2	λ	12	/	/
Converters parameters				Solver	
Boost		Buck boost	Bidirectional converter	solver type	duration
L = 0.07 H		L= 40 mH	L=0.01 H	Fixed-step	7.5 sec
		C_{in}= 0.1 mF	C_{in} = 0.1 mF	/	/

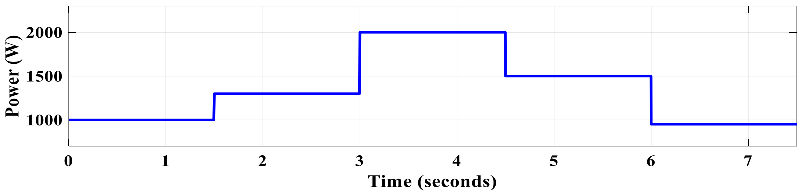

Figure 6. Load profile

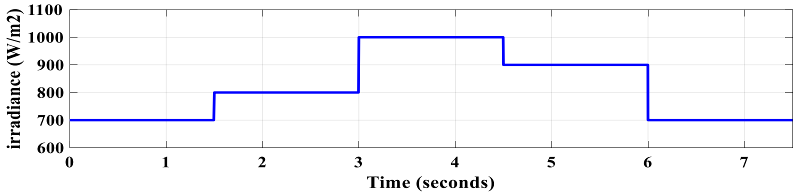

Figure 7. Irradiance profile

5.1. Case 1: $SOC < SOC_{min}$

The power that is produced by each source is shown in Figure 8, along with the states that correspond to the functioning of the system that is shown in Table 2. Figure 8(a) shows the operational outcomes when the battery's SOC is below SOCmin, and Figure 8(b) depicts the states produced from case one. The power generated by the photovoltaic system is less than the power demand. When the SOC drops below the minimum value, additional charging is needed to restore the battery's charge level. The PEMFC must both compensate for the power shortfall and recharge the battery, the initial SCO equal to 20%, State 1, from 0s to 1.5s and 6s to 7s, the PV generated a power not satisfied the load demand; concurrently, the PEMFC driver the rest of the load requirement, while the remainder was used to charge the battery. State 2 denoted the time interval from 1.5s to 3s and 4.5s to 6s the PEMFC driver provided a total power that meet the load demanded and charge the battery. During the state 3, occurring within the time frame of 4.5s to 6s, also the PEMFC charge the battery and meet the load demand.

While the DC bus voltage and the SOC of the battery bank are displayed in Figure 9, Figure 9(a) depicts the DC link voltage, with the reference value set at 180 W. The bus voltage accurately follows the reference, with peaks at 1.5s, 3s, 4.5s, and 6s resulting from fluctuations in load demand. A divergence from the reference is noted, followed by a swift reversion to the reference value. Figure 9(b) illustrates the SOC of the batteries, indicating that the batteries are charging regardless of the load demand. The power generated by the PEMFC system provides energy to the load while simultaneously charging the batteries, as their SOC < SOCmin. Figure 10 displays the power output of the PEMFC utilizing the proposed SMC-SMCC in contrast to the conventional SMC-PI; the graphic demonstrates that the recommended energy management technique yields superior results, which are encapsulated in the accompanying Table 4.

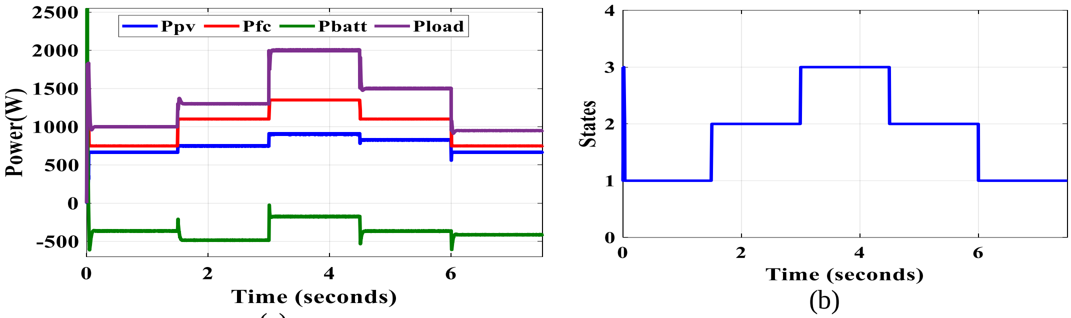

Figure 8. Power generation and operating state of the proposed energy management system under the condition $SOC < SOC_{min}$: (a) power generated by the PV, PEMFC, and battery, and (b) corresponding operating states

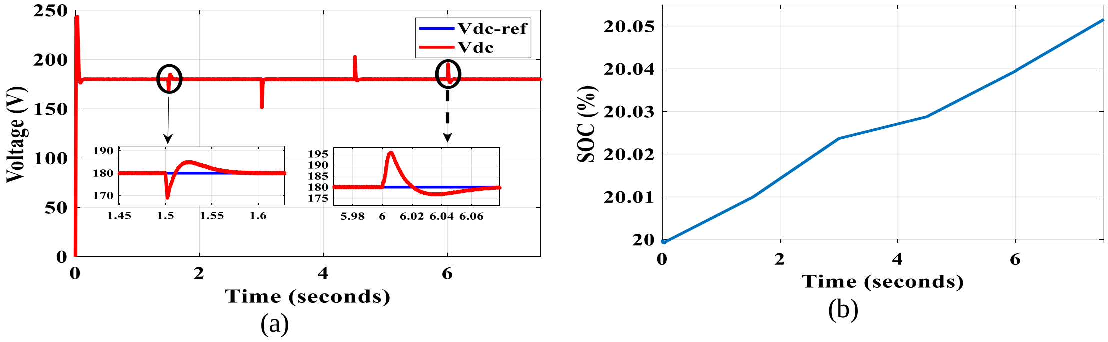

Figure 9. Electrical performance of the proposed system under the condition $SOC < SOC_{min}$: (a) DC bus voltage response and (b) battery state of charge (SOC)

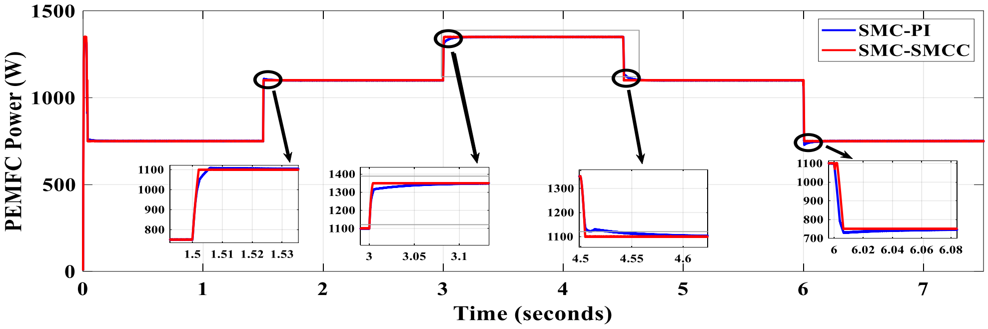

Figure 10. Comparison between different controllers ($SOC < SOC_{min}$)

Table 4. Response time comparison of different controllers

	Interval	SMC-PI	SMC-SMCC
Response time (s)	0 - 1.5s	0.17	0.06s
	1.5s - 3s	0.35	0.07
	3s - 4.5s	0.2	0.004
	4.5s - 6s	0.24	0.0045s
	6s - 7.5s	0.25	0.0065

5.2. Case 2: $SOC_{min} < SOC < SOC_{max}$

The battery SOC is considered to be above the minimum permissible SOC and below the maximum SOC. In this case, the surplus energy produced by the photovoltaic system is stored in the battery storage system, also feeding the load demand, depending on the state. Regarding the case 2. The output generated by each source is illustrated in Figure 11, alongside the states corresponding to the system's operation as detailed in Table 2. Figures 11(a) and 11(b) illustrates the power generated from the sources, and depicts the corresponding state for this scenario. The time intervals [0s 1.5s] and [6s 7.5s] correspond to state number four, the photovoltaic (PV) system produces maximum power, while the PEMFC supplies the load with maximum power (Pmax), and the surplus power charges the battery. State number five encompasses the time intervals from 1.5s to 3s and from 4.5s to 6s, the PV does not generate sufficient electricity to meet load requirements; consequently, the PEMFC compensates for the energy deficit to the load. In state number six, corresponding to the time interval [3s 4.5s], the photovoltaic system produces insufficient power to meet the load demand; hence, the PEMFC and the battery supply the deficit power required by the load.

The DC bus voltage and the current SOC of the battery bank are both displayed in Figure 12. Figure 12(a) illustrates the DC link voltage, with a reference value of 180W. The bus voltage closely tracks the reference, with peaks at 1.5s, 3s, 4.5s, and 6s caused by load demand fluctuations. A deviation from the reference is observed, followed by a quick return to the reference value. Figure 12(b) illustrates the SOC from 0s to 7s. The battery's initial values are 66%. The SOC fluctuates between 66.025% and 65.996%, indicating that battery charging and discharging are contingent upon load demand and the power output of the PEMFC at the corresponding condition. Figure 13 compares the power output of PEMFCs utilizing the conventional SMC-PI and the new SMC-SMCC energy management method; the findings are summarized in the Table 5, and the figure shows that the new strategy produces better responses.

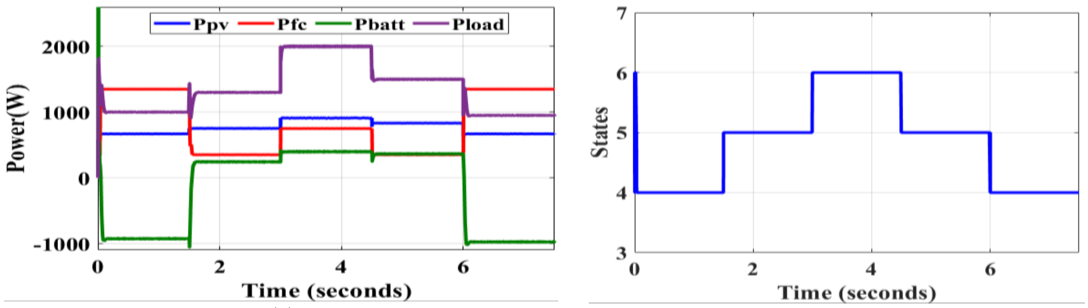

(a) (b)

Figure 11. Power generation and operating state of the proposed energy management system under the condition $SOC_{min} < SOC < SOC_{max}$: (a) power generated by the PV, PEMFC, and battery, and (b) corresponding operating states

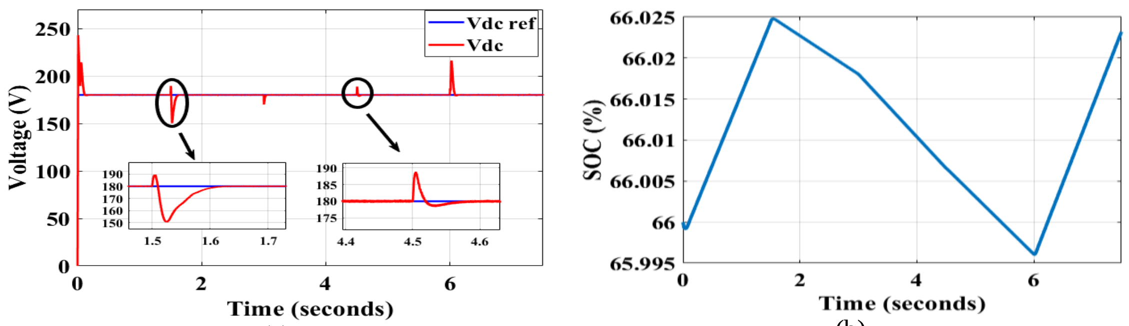

(a) (b)

Figure 12. Electrical performance of the proposed system under the condition $SOC_{min} < SOC < SOC_{max}$: (a) DC bus voltage response and (b) battery state of charge (SOC)

Table 5. Response time comparison of different controllers

	Interval	SMC-PI	SMC-SMCC
Response time (s)	0 – 1.5 s	0.34	0.045
	1.5s -3 s	0.45	0.05
	3s -4.5s	0.3	0.0015
	4.5s- 6s	0.35	0.0061
	6 s- 7.5s	0.345	0.01

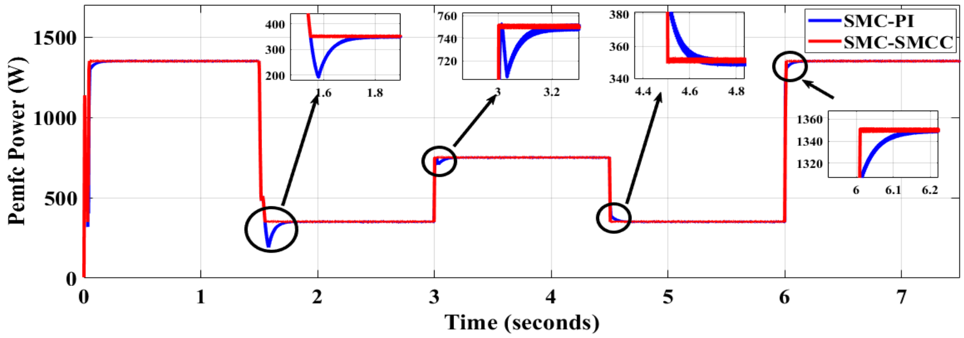

Figure 13. Comparison between different controllers ($\mathrm{SOC_{min}} < \mathrm{SOC} < \mathrm{SOC_{max}}$)

5.3. Case 3 $\mathbf{SOC > SOC_{max}}$

This mode activates when the battery is fully charged. The SOC exceeds the maximum value. Additionally, the battery will deplete, and the PEMFC will operate at minimal power. This indicates that the system relies on the BEES' backup. Given the case 3. Figure 14 shows the output from each source, and Table 2 details the states that correlate to the system's operation. Figures 14(a) and 14(b) demonstrates the power produced by the sources and represents the associated state for this situation. The time intervals [0s 1.5s] and [6s 7.5s] pertain to state number seven, during which the photovoltaic (PV) system generates peak electricity. The PEMFC concurrently provides the load with the minimal power Pmax, while the excess power drains the battery because the battery's SOC exceeds the maximum threshold. State number 8 encompasses the time intervals from 1.5s to 3s and from 4.5s to 6s; during this duration, the photovoltaic system fails to provide sufficient electricity to satisfy load requirements; consequently, the proton exchange membrane fuel cell provides a little amount of power for compensation, while the battery compensates for the remainder. In state number 9, throughout the time interval [3s 4.5s], the photovoltaic system generates inadequate power to satisfy the load demand; hence, the battery compensates for the deficiency, supplemented by a minimal contribution from the PEMFC, equating to the minimum (Pmin).

Figure 15 shows the DC bus voltage and the battery bank's charge status. Figure 15(a) shows the DC link voltage, with a reference value of 180W. The bus voltage closely follows the reference, with peaks at 1.5s, 3s, 4.5s, and 6s caused by load demand changes. A deviation from the reference occurs, followed by a quick return to the reference value. Figure 15(b) displays the SOC from 0s to 7.5s. The battery initially starts at 92% charge. The SOC fluctuates between 92% and 91.955%, indicating that battery discharging due to the initial SOC is above the SOCmax.

The power output of PEMFCs that use the standard SMC-PI energy management approach and the novel SMC-SMCC energy management method are compared in Figure 16. The response time for each state, are summarized in Table 6, and the figure demonstrates that the new strategy delivers better responses than the conventional management method. Finally, Table 7 tables by highlighting key improvements of the proposed SMC-SMCC time reduction, SOC stability, and overshoot.

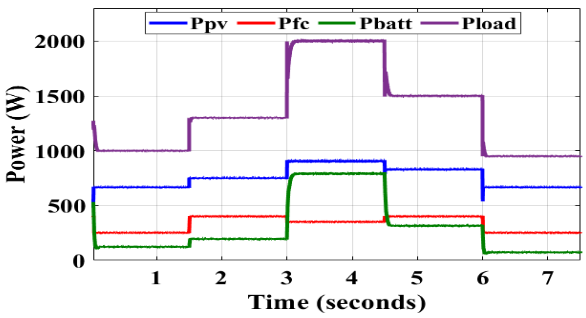

(a)

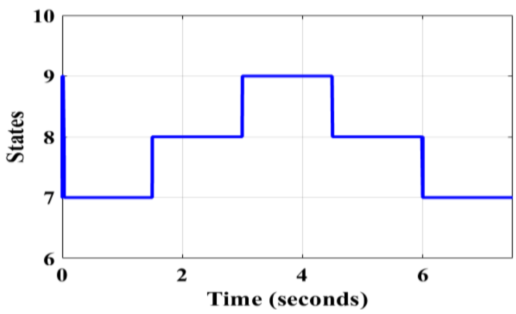

(b)

Figure 14. Power generation and operating state of the proposed energy management system under the condition $SOC > SOC_{max}$: (a) power generated by the PV, PEMFC, and battery and (b) corresponding operating states

Table 6. Response time comparison of different controllers

	Interval	SMC-PI	SMC-SMCC
Response time (s)	0 - 1.5s	0.4	0.0417
	1.5s - 3s	0.035	0.0045
	3s - 4.5s	0.0014	0.0014
	4.5s - 6s	0.0018	0.0001645
	6s - 7.5s	0.08	0.0053

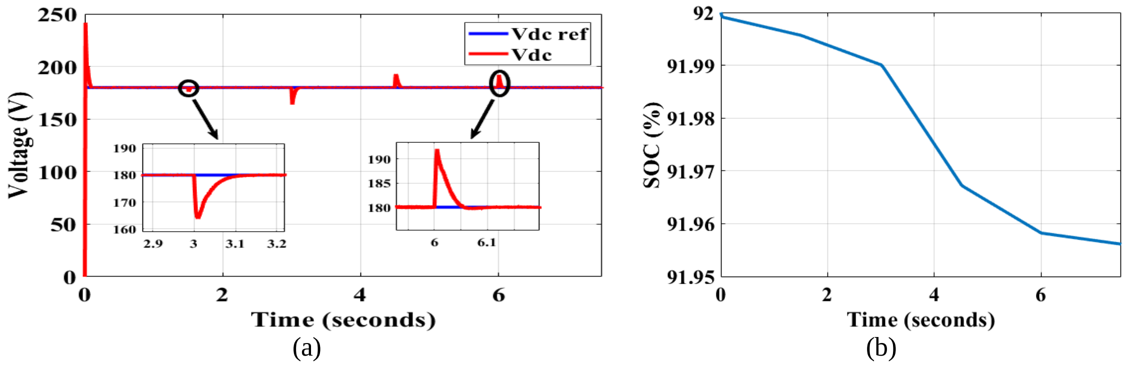

Figure 15. Electrical performance of the proposed system under the condition $SOC > SOC_{max}$: (a) DC bus voltage response and (b) battery state of charge (SOC)

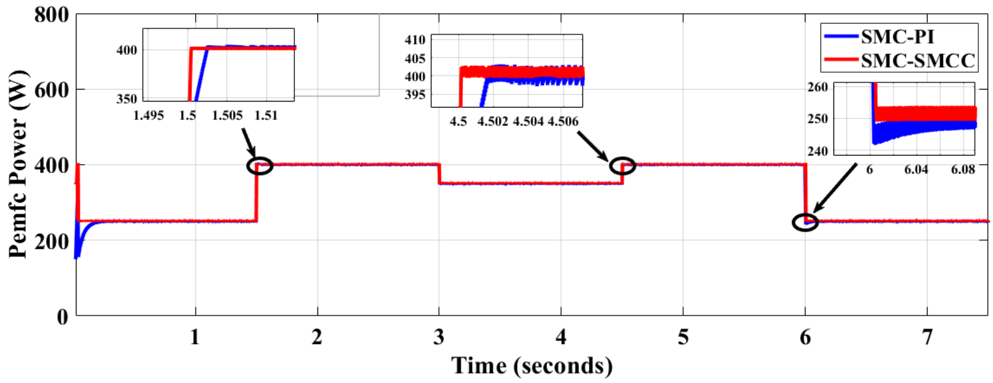

Figure 16. Comparison between different controllers ($SOC > SOC_{max}$)

Table 7. Comparison between SMC-PI and SMC-SMCC

Metric	SMC-PI	SMC-SMCC
Response time	Slow	Fast
SOC stability	Fluctuating	Stable
Overshoot	Higher	Lower

6. CONCLUSION

This research introduces novel energy management algorithms designed exclusively for DC microgrids, emphasizing efficient power management and the provision of local loads. In multi-source DC microgrid settings, integrating SMC-SMCC-based energy management systems with nine states significantly enhances the stability, efficacy, and responsiveness of the controllers. A comprehensive examination of DC-DC converters and the optimization of power distribution between sources and loads highlights the efficacy of these approaches. The suggested SMC-SMCC controller demonstrates superiority over standard SMC-PI controllers, particularly regarding time response, as evidenced by rigorous comparative analysis. The proposed energy management controller for multi-source DC microgrids is an SMC-based SMCC system that outperforms conventional SMC-PI controllers in terms of response time, efficiency, and stress reduction. It also provides substantial benefits in improving system reliability and longevity. The real-world application of sliding mode control may face issues including chattering, sensitivity to measurement noise, and the necessity for meticulous parameter tweaking, despite its high durability and rapid dynamic response. These concerns are substantial, and they are on top of the operational limitations and deployment considerations. Future work will focus on a comprehensive sensitivity analysis to quantify the influence of critical design and control parameters on overall system performance, stability, and robustness. Particular attention will be given to SOC thresholds (upper/lower bounds and hysteresis margins) to assess their impact on power-sharing behavior, battery degradation, and cycling stress. Furthermore, the sensitivity of converter-related parameters—such as switching frequency, passive component values, DC-link voltage reference, and controller tuning gains—will be systematically evaluated with respect to efficiency, dynamic response, and stability margins. The outcomes of this study will strengthen the robustness of the proposed EMS and establish reliable design guidelines under parameter uncertainties and realistic operating conditions.

ACKNOWLEDGMENTS

I would like to express my gratitude and appreciation for LAS members. whose guidance, supportand encouragement has been invaluable throughout this study.

FUNDING INFORMATION

Authors state no funding involved.

AUTHOR CONTRIBUTIONS STATEMENT

This journal uses the Contributor Roles Taxonomy (CRediT) to recognize individual author contributions, reduce authorship disputes, and facilitate collaboration.

Name of Author	C	M	So	Va	Fo	I	R	D	O	E	Vi	Su	P	Fu
Hamza Rezigue	✓	✓	✓	✓	✓	✓		✓	✓	✓	✓		✓	
Mabrouk Khemliche		✓				✓		✓	✓	✓	✓	✓		
Samia Latreche	✓		✓	✓			✓			✓	✓		✓	✓
Badreddine Kanouni			✓	✓		✓				✓	✓		✓	✓
Hamza Khemliche			✓		✓		✓			✓		✓		✓

C : **C**onceptualization	I : **I**nvestigation	Vi : **Vi**sualization
M : **M**ethodology	R : **R**esources	Su : **Su**pervision
So : **So**ftware	D : **D**ata Curation	P : **P**roject administration
Va : **Va**lidation	O : Writing - **O**riginal Draft	Fu : **Fu**nding acquisition
Fo : **Fo**rmal analysis	E : Writing - Review & **E**diting	

CONFLICT OF INTEREST STATEMENT

Authors state no conflict of interest.

DATA AVAILABILITY

Data availability is not applicable to this paper as no new data were created or analyzed in this study.

REFERENCES

[1] H. Feroura, F. Krim, B. Tabli, and A. Laib, "Finite-set model predictive voltage control for islanded three phase current source inverter," in *2017 5th International Conference on Electrical Engineering - Boumerdes, ICEE-B 2017*, IEEE, Oct. 2017, pp. 1–5. doi: 10.1109/ICEE-B.2017.8192100.

[2] S. Latreche, A. Bouafassa, B. Babes, and O. Aissa, "Efficient Dsp-based real-time implementation of anfis regulator for single-phase power factor corrector," *Revue Roumaine des Sciences Techniques Serie Electrotechnique et Energetique*, vol. 69, no. 2, pp. 141–146, Jul. 2024, doi: 10.59277/RRST-EE.2024.2.4.

[3] A. Laib, F. Krim, B. Talbi, H. Feroura, and A. Kihal, "Decoupled active and reactive power control strategy of grid-connected six-level diode-clamped inverters based on finite set model predictive control for photovoltaic application," *Revue Roumaine des Sciences Techniques Serie Electrotechnique et Energetique*, vol. 64, no. 1, pp. 51–56, 2019.

[4] S. Remache, S. E. I. Remache, A. Y. Cherif, K. Barra, and E. Kabalci, "Improved power management of standalone DC microgrid with hybrid energy storage system using a fixed switching frequency model predictive control," *International Journal of Circuit Theory and Applications*, vol. 54, no. 3, pp. 1446–1460, Mar. 2026, doi: 10.1002/cta.70039.

[5] G. Van den Broeck, J. Stuyts, and J. Driesen, "A critical review of power quality standards and definitions applied to DC microgrids," *Applied Energy*, vol. 229, pp. 281–288, Nov. 2018, doi: 10.1016/j.apenergy.2018.07.058.

[6] S. R. Hukampal, P. Jena, and D. K. Singh, "Real-time energy management system for standalone and grid-connected hybrid AC/DC microgrid," *IEEE Journal of Emerging and Selected Topics in Power Electronics*, vol. 14, no. 2, pp. 2369–2382, Apr. 2025, doi: 10.1109/JESTPE.2025.3619661.

[7] B. Kanouni, A. E. Badoud, S. Mekhilef, M. Bajaj, and I. Zaitsev, "Advanced efficient energy management strategy based on state machine control for multi-sources PV-PEMFC-batteries system," *Scientific Reports*, vol. 14, no. 1, p. 7996, Apr. 2024, doi: 10.1038/s41598-024-58785-2.

[8] R. Sepehrzad, A. Hedayatnia, M. Amohadi, J. Ghafourian, A. Al-Durra, and A. Anvari-Moghaddam, "Two-stage experimental intelligent dynamic energy management of microgrid in smart cities based on demand response programs and energy storage system participation," *International Journal of Electrical Power and Energy Systems*, vol. 155, p. 109613, Jan. 2024, doi: 10.1016/j.ijepes.2023.109613.

[9] R. P. Kumar and G. Karthikeyan, "A multi-objective optimization solution for distributed generation energy management in microgrids with hybrid energy sources and battery storage system," *Journal of Energy Storage*, vol. 75, p. 109702, Jan. 2024, doi: 10.1016/j.est.2023.109702.

[10] A. Laib, F. Krim, B. Talbi, H. Feroura, and A. Belaout, "Hardware implementation of fuzzy maximum power point tracking through sliding mode current control for photovoltaic systems," *Revue Roumaine des Sciences Techniques Serie Electrotechnique et Energetique*, vol. 66, no. 2, pp. 91–96, 2021.

[11] Y. Li, J. Tao, L. Xie, R. Zhang, L. Ma, and Z. Qiao, "Enhanced Q-learning for real-time hybrid electric vehicle energy management with deterministic rule," *Measurement and Control (United Kingdom)*, vol. 53, no. 7–8, pp. 1493–1503, 2020, doi: 10.1177/0020294020944952.

[12] S. Siddula, "Fuzzy based energy management strategy for battery and fuel cell hybrid vehicles," in *Proceedings of ICWITE 2024: IEEE International Conference for Women in Innovation, Technology and Entrepreneurship*, IEEE, Feb. 2024, pp. 637–641. doi: 10.1109/ICWITE59797.2024.10502426.

[13] P. Cui, A. Ding, Y. Shen, and Y. X. Wang, "Hybrid fuel cell/battery power system energy management by using fuzzy logic control for vehicle application," in *2019 3rd IEEE International Conference on Green Energy and Applications, ICGEA 2019*, IEEE, Mar. 2019, pp. 132–135. doi: 10.1109/ICGEA.2019.8880770.

[14] S. Luciani and A. Tonoli, "Control strategy assessment for improving PEM fuel cell system efficiency in fuel cell hybrid vehicles," *Energies*, vol. 15, no. 6, p. 2004, Mar. 2022, doi: 10.3390/en15062004.

[15] H. F. Ghavidel and S. M. Mousavi-G, "Modeling analysis, control, and type-2 fuzzy energy management strategy of hybrid fuel cell-battery-supercapacitor systems," *Journal of Energy Storage*, vol. 51, p. 104456, Jul. 2022, doi: 10.1016/j.est.2022.104456.

[16] R. Zhang, J. Tao, and H. Zhou, "Fuzzy optimal energy management for fuel cell and supercapacitor systems using neural network based driving pattern recognition," *IEEE Transactions on Fuzzy Systems*, vol. 27, no. 1, pp. 45–57, Jan. 2019, doi: 10.1109/TFUZZ.2018.2856086.

[17] S. Alghamdi, M. Alqarni, M. R. Hammad, and K. M. AboRas, "First-of-its-kind frequency enhancement methodology based on an optimized combination of FLC and TFOIDFF controllers evaluated on EVs, SMES, and UPFC-integrated smart grid," *Fractal and Fractional*, vol. 7, no. 11, p. 807, Nov. 2023, doi: 10.3390/fractalfract7110807.

[18] S. Necaibia *et al.*, "A combined multi-trial vector-based sine cosine optimization and integral derivative sliding mode control for photovoltaic systems under partial shading conditions," in *Conference Record - IAS Annual Meeting (IEEE Industry Applications Society)*, IEEE, Jun. 2025, pp. 1–6. doi: 10.1109/IAS62731.2025.11061561.

[19] K. Bouguerra, S. Latreche, M. Khemliche, and H. Khemlche, "Modeling and simulation of a photovoltaic system using a synergistic control and (INC), (P&O) connected to a load and to an electric grid," in *2024 International Conference on Advances in Electrical and Communication Technologies, ICAECOT 2024*, IEEE, Oct. 2024, pp. 1–7. doi: 10.1109/ICAECOT62402.2024.10828898.

[20] K. Bouguerra, S. Latreche, H. Khemliche, and M. Khemliche, "Pv system mppt control: a comparative analysis of P&O, Inccond, Smc and Flc algorithms," *Informatyka, Automatyka, Pomiary w Gospodarce i Ochronie Srodowiska*, vol. 14, no. 4, pp. 52–62, 2024, doi: 10.35784/iapgos.6152.

[21] B. Kanouni, A. Laib, A. Krama, S. Necaibia, and J. M. Guerrero, "Horned lizard defense tactics optimization algorithm for precise identification of PEMFC parameters," *Fuel Cells*, vol. 25, no. 4, Aug. 2025, doi: 10.1002/fuce.70011.

[22] B. Babes *et al.*, "A dSPACE-based implementation of ANFIS and predictive current control for a single phase boost power factor corrector," *Scientific Reports*, vol. 14, no. 1, p. 12775, Jun. 2024, doi: 10.1038/s41598-024-63740-2.

[23] A. Kihel, F. Krim, and A. Laib, "MPPT voltage oriented loop based on integral sliding mode control applied to the boost converter," in *2017 6th International Conference on Systems and Control (ICSC)*, IEEE, May 2017, pp. 205–209. doi: 10.1109/ICoSC.2017.7958687.

[24] A. Laib, F. Krim, B. Talbi, A. Kihal, and H. Feroura, "Improved control of three phase dual-stage grid-connected PV system based on a predictive control strategy," *Control Engineering and Applied Informatics*, vol. 20, no. 3, pp. 12–23, 2018.

[25] S. Latreche, B. Babes, and A. Bouafassa, "Design and real-time implementation of synergetic regulator for a Dc-Dc boost converter," *Revue Roumaine des Sciences Techniques Serie Electrotechnique et Energetique*, vol. 69, no. 3, pp. 309–315, 2024, doi: 10.59277/RRST-EE.2024.69.3.9.

BIOGRAPHIES OF AUTHORS

Hamza Rezigue was born was bom in Setif town – Algeria. He is Ph.D. Student at Automatic Laboratory, Electrical Engineering Department, Faculty of Technology, University of Setif1 (Algeria). His main research areas concern Modeling and Monitoring of concrete plant using the bond graph tool and online validation by a SCADA system and Contribution to the supervision of industrial systems. He can be contacted at email: rezigue.hamza@gmail.com.

Prof. Mabrouk Khemliche was born in Setif - Algeria. He is, since 2012, Professor at Electrical Engineering Department of Setif (Algeria). He heads the Automatic Laboratory of Setif-LAS and the Monitoring team of LAS laboratory. His main research areas concern Diagnosis and Control in Electrical and Process Engineering systems using new technologies, artificial intelligence by analytical and graphical approaches. Their application domains are mainly nuclear, renewable energy, thermo fluid and petrochemical processes. He is the author of more than 150 international publications and communications. He can be contacted at email: mabroukkhemliche@univ-setif.dz.

Samia Latreche was born in Setif town - Algeria. She is, since 2016, a Ph.D. at Automatic Laboratory, Electrical Engineering Department, Faculty of Technology, University of Setif (Algeria), she obtained the HDR Degree in 2019. Her main research concern Control, Fault Detection and Isolation, identification-based diagnosis. The application domains are mainly Process Engineering, Renewable Energies and Power Systems. Her main research concern Fault Detection and Isolation, identification-based diagnosis. The domain application is mainly Process Engineering and renewable energies. She is the author of 29 publications and 90 international communications. She can be contacted at email: ksamia2002@yahoo.fr.

Badreddine Kanouni holds a Ph.D. in Automatic Control from the University of Ferhat Abbas Setif-1, Algeria. He obtained his bachelor's and master's degrees in industrial electronics from the University of Ferhat Abbas Setif-1, Algeria, in 2014 and 2016, respectively. His research interests include advanced control, control strategies, multilevel inverters, optimization, energy management strategies, and renewable energy sources. He can be contacted at email: badreddine.kanouni@univ-setif.dz.

Mr. Hamza Khemliche was born in Setif - Algeria. He is senior research engineer at the Research Center in Industrial Technologies -CRTI- (Algeria). He is head of the IT cell at the additive manufacturing research unit –URFA-. His main research areas concern Simulation, Modeling and Monitoring of Computer Science Systems. Their application domains are sensor networks, renewable energy and additive manufacturing. He is the author of many international publications and communications. He can be contacted at email: h.khemliche@crti.dz.